High-Affinity Metal-Binding Site in Beef Heart Mitochondrial F_1ATPase: An EPR Spectroscopy Study†

Alfonso Zoleo,‡ Stefania Contessi,§,|| Giovanna Lippe,§,|| Luca Pinato,‡ Marina Brustolon,‡ Louis Claude Brunel,⊥ Federica Dabbeni-Sala,*,# and Anna Lisa Maniero*,‡

Department of Chemistry, University of Padova, via Marzolo 1, I-35131 Padova, Italy, Department of Biomedical Sciences and Technologies, University of Udine, P.le Kolbe 4, I-33100 Udine, Italy, MATI Center of Excellence, University of Udine, P.le Kolbe 4, I-33100 Udine, Italy, Center for Interdisciplinary Magnetic Resonance, National High Magnetic Field Laboratory, Florida State University, 1800 East Paul Dirac Drive, 32310 Tallahassee, Florida, and Department of Pharmacology, University of Padova, Largo Meneghetti 2, I-35131 Padova, Italy

Received March 10, 2004; Revised Manuscript Received July 19, 2004

ABSTRACT: The high-affinity metal-binding site of isolated F_1-ATPase from beef heart mitochondria was studied by high-field (HF) continuous wave electron paramagnetic resonance (CW-EPR) and pulsed EPR spectroscopy, using Mn^{II} as a paramagnetic probe. The protein F_1 was fully depleted of endogenous Mg^{II} and nucleotides [stripped F_1 or MF1(0,0)] and loaded with stoichiometric Mn^{II} and stoichiometric or excess amounts of ADP or adenosine 5′-(β,γ-imido)-triphosphate (AMPPNP). Mn^{II} and nucleotides were added to MF1(0,0) either subsequently or together as preformed complexes. Metal-ADP inhibition kinetics analysis was performed showing that in all samples Mn^{II} enters one catalytic site on a β subunit. From the HF-EPR spectra, the zero-field splitting (ZFS) parameters of the various samples were obtained, showing that different metal-protein coordination symmetry is induced depending on the metal nucleotide addition order and the protein/metal/nucleotide molar ratios. The electron spin-echo envelope modulation (ESEEM) technique was used to obtain information on the interaction between Mn^{II} and the ^{31}P nuclei of the metal-coordinated nucleotide. In the case of samples containing ADP, the measured ^{31}P hyperfine couplings clearly indicated coordination changes related to the metal nucleotide addition order and the protein/metal/nucleotide ratios. On the contrary, the samples with AMPPNP showed very similar ESEEM patterns, despite the remarkable differences present among their HF-EPR spectra. This fact has been attributed to changes in the metal-site coordination symmetry because of ligands not involving phosphate groups. The kinetic data showed that the divalent metal always induces in the catalytic site the high-affinity conformation, while EPR experiments in frozen solutions supported the occurrence of different precatalytic states when the metal and ADP are added to the protein sequentially or together as a preformed complex. The different states evolve to the same conformation, the metal^{II}−ADP inhibited form, upon induction of the trisite catalytic activity. All our spectroscopic and kinetic data point to the active role of the divalent cation in creating a competent catalytic site upon binding to MF1, in accordance with previous evidence obtained for *Escherichia coli* and chloroplast F_1.

Mg^{2+} cations generally act as co-activators of a large variety of enzymes that use nucleotides as substrates. Among these enzymes, the F_0-F_1 ATP[1] synthase catalyses the reversible synthesis of ATP from ADP and P_i, a ubiquitous energy-rich molecule that is involved in many cellular energetic processes. ATP synthesis and hydrolysis occur in nucleotide-binding sites located on the F_1 sector. F_1 may be easily detached from the membrane-embedded F_0 sector, and it acts as an ATPase catalyzing hydrolysis of ATP to ADP and P_i.

The F_1 moiety is composed of five different subunits (α_3, β_3, γ, δ, and ϵ); it contains six nucleotide-binding sites. Three of them, mainly located on three β subunits, participate in catalysis. The occupancy of all three catalytic sites by nucleotides (trisite catalysis) is the required mode of operation to achieve physiological rates. A much lower turnover is achieved upon addition of a stoichiometric nucleotide; this

† This work was supported by the University of Padova through the project "Studio con risonanze di Spin elettronico dell'enzima F1" (Cdr. A.0EE00.96) and through the Grant "Assegno di Ricerca 2001" prot. CPDR011922.

* To whom correspondence should be addressed. Telephone: +39-049-8275096. Fax: +39-049-8275093. E-mail: federica.dabbenisala@unipd.it (F.D.-S.); Telephone: +39-049-8275109. Fax: +39-049-8275239. E-mail: a.maniero@chfi.unipd.it (A.L.M.).

‡ Department of Chemistry, University of Padova.

§ Department of Biomedical Sciences and Technologies, University of Udine.

|| MATI Center of Excellence, University of Udine.

⊥ Florida State University.

Department of Pharmacology, University of Padova.

[1] Abbreviations: ADP, adenosine 5′-diphosphate; AMPPNP, adenosine 5′-(β,γ-imido)-triphosphate; ATP, adenosine 5′-triphosphate; EDTA, ethylenediaminetetraacetic acid; PEP, phosphoenolpyruvate; EPR, electron paramagnetic resonance; ESEEM, electron spin-echo envelope modulation; HF-EPR, high-field EPR; ZFS, zero-field splitting; HYSCORE, hyperfine sublevel correlation spectroscopy; MF1, F_1 H^+-ATPase from bovine heart mitochondria; TF1, F_1 H^+-ATPase from thermophilic *Bacillus* PS3; CF1, F_1 H^+-ATPase from chloroplast.

10.1021/bi049525k CCC: $27.50
Published on Web 09/25/2004

operation mode is defined as unisite catalysis and involves a single occupied site operating alone (*1*). The three other nucleotide-binding sites are noncatalytic with a much less clear function. They are located on α subunits with contribution of some residues from adjacent *β* subunits. F_1 enzymes have been purified from a variety of organisms and organelles including bacteria, mitochondria, and chloroplasts. The X-ray 3D structure of bovine heart mitochondrial F_1 enzyme (MF1) has been determined at atomic resolution (*2*) and used as a basic model to study also F_1 from bacteria and chloroplasts. F_1 has in fact conserved α_3, β_3, and γ subunits (*3*), while δ and ϵ have a different function and structure in the different organelles and organisms (*1*, *4*, *5*).

As mentioned above, ATP synthase and isolated F_1 necessitate the presence of divalent metal cations for their enzymatic reactions. The current model sustains that the true substrate of ATP synthesis and hydrolysis is the complex Mg^{II}−nucleotide; however, some researchers consider the divalent cation Mg^{2+} as an activator and the nucleotide as the true substrate (*6*, *7*).

Several studies show evidence that Mg^{2+} ions are responsible for large differences in nucleotide affinities (*8*, *9*). In the absence of Mg^{2+}, all three catalytic sites bind free ATP or ADP with low affinity and there is no catalysis. In the presence of Mg^{2+}, pronounced binding cooperation among the three catalytic sites is observed (*9*). It is a basic tenet of all current models of the mechanism that only one catalytic site is catalytically competent, and as shown in *Escherichia coli* F_1 (*8*), this site is formed in the high-affinity state only in the presence of Mg^{2+}.

In the MF1 crystal structure, Mg^{2+} cations are associated to the five occupied nucleotide sites with either ADP or adenosine 5′-(*β*,*γ*-imido)-triphosphate (AMPPNP) molecules, the latter one being a nonhydrolysable ATP analogue. The *β* phosphate of ADP and both *β* and *γ* phosphate groups of AMPPNP serve as ligands to the bound Mg^{2+} cofactors. However, other ligands derived from amino acid residues in the α and *β* subunits are involved in binding Mg^{2+}. The Mg^{2+} ions present in two catalytic sites are coordinated by the hydroxyl oxygen of *β*-Thr163 as inferred by the average distance of 2.1 Å between the Mg^{2+} ion and the coordinated oxygen. The other Mg^{2+} ligands are not clearly identified and are presumably water molecules. On the contrary, the coordination of Mg^{2+} appears to be similar in the three noncatalytic sites, which are occupied by AMPPNP molecules (*2*).

The Mg^{2+} ion has a strong tendency to assume an octahedral coordination; thus, only metal cations able to assume the same coordination and with a comparable ionic radius, such as Mn^{2+}, Co^{2+}, and Zn^{2+}, could be cofactors of ATPase hydrolytic activity (*10*). Among divalent cations that could replace the natural Mg^{2+} in the ATP hydrolysis reaction, Mn^{2+} and VO^{2+} are of special interest because of their paramagnetic properties that can be investigated by continuous wave electron paramagnetic resonance (CW-EPR) and pulsed EPR techniques, such as electron spin-echo envelope modulation (ESEEM). EPR techniques have been used to study the binding site(s) of the metal cation in F_1 from different sources and in particular to investigate the specific metal−nucleotide interaction in enzymes from thermophilic bacteria PS3 (TF1) and from chloroplast (CF1) (*11*−*14*).

In the present study, we have extended this approach to study the interaction of stoichiometric Mn^{2+} with beef heart mitochondrial F_1, fully depleted of Mg^{2+} and nucleotides [MF1(0,0) or stripped], in the absence or in the presence of a controlled amount of added nucleotides. No crystal structure of this fully depleted enzyme is available. The metal cation Mn^{2+} has been added to the stripped enzyme in two ways, by preloading with Mn^{2+} and the subsequent addition of the nucleotide in 1:1 or 10:1 ratio with respect to the metal or by adding the precoordinated (1:1) Mn^{II}−nucleotide complex. In our investigation, we combined two different approaches, metal−ADP inhibition kinetics analysis and EPR spectroscopy. The inhibition kinetic analyses using Mg^{2+}/Mn^{2+} and ADP were performed to confirm that the subunit, which interacts with stoichiometric Mn^{2+}, is one catalytic *β* subunit. In fact, it is well-known that sequential treatment of stripped F_1 with Mg^{2+} and a stoichiometric amount of ADP induces a catalytic site in the final high-affinity β_{ADP} conformation, resulting in the generation of the so-called MgADP-inhibited form (*15*, *16*).

As already mentioned, EPR is a useful technique for investigating the binding of paramagnetic metals in enzymes, because the typical EPR parameters, such as hyperfine couplings, g factors, and zero-field splitting (ZFS) parameters, are very sensitive to the environment around the metal center (*17*). Specifically, for Mn^{II} complexes, CW-EPR spectra allow for the obtaining of ZFS parameters and the hyperfine-coupling constant of the ^{55}Mn nucleus, both providing information on the Mn^{2+} coordination. However, the CW-EPR spectra of Mn^{II} complexes, at the normally used microwave frequency (9.5 GHz, X band), are strongly influenced by high-order effects, making any simulation difficult (*18*). For this reason, we have recorded high-field EPR (HF-EPR) spectra at the W band (95 GHz), that can be easily interpreted, because these high-order effects, which reflect the relative magnitude of the ZFS with respect to the microwave frequency, strongly decrease at frequencies higher than the X band (*19*−*23*). The ESEEM technique is a valuable method to obtain detailed information on small hyperfine couplings of long-range nuclei. This technique has been used in the present study to investigate the interaction of the Mn^{2+} ion with magnetic nuclei belonging to the surrounding ligands, in particular the ^{31}P nuclei of the nucleotides coordinating the Mn^{2+} (*24*).

We obtained distinctive HF-EPR and ESEEM spectra, providing clear evidence of different metal−protein coordinations for samples prepared by adding to the stripped MF1 metal and nucleotides in different molar ratios and different addition orders. All our spectroscopic results substantiate the different approach of the metal−nucleotide complexes to the enzyme with respect to the metal alone and support the hypothesis of Senior et al. on the conformational role of Mg^{2+} ion in the induction of a competent catalytic site (*8*, *9*).

EXPERIMENTAL PROCEDURES

Purification of MF1. Salts and buffers were from Sigma−Aldrich. ATP, ADP, and AMPPNP were from ICN. Pyruvate kinase, lactate dehydrogenase, NADH, and PEP (phosphoenolpyruvate) were from Roche. Pure soluble MF1 was prepared from beef heart mitochondria as in ref *25*. Nucleotide and Mg-depleted MF1 (stripped MF1) was obtained

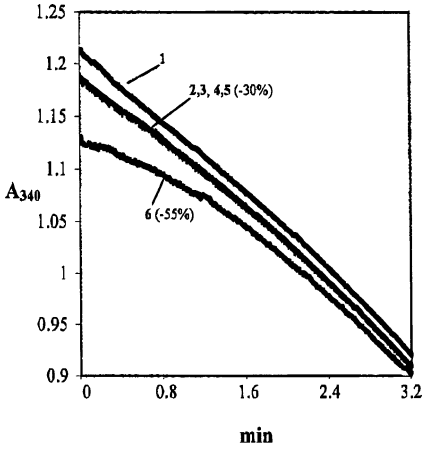

FIGURE 1: Activity measurements: curve 1, 2.2 μM stripped F_1 dissolved in 20 mM Tris/HCl and 20% (v/v) glycerol at pH 7.4, incubated for 15 min at 37 °C; curves 2 and 3, MF1 preincubated in the buffer at 37 °C for 5 min with 2.2 μM metal (Mg^{2+} or Mn^{2+}), followed by 10 min of incubation with added 2.2 μM ADP; curves 4 and 5 (exactly superimposed to curves 2 and 3), MF1 preincubated in the buffer at 37 °C for 15 min with 2.2 μM metal−ADP complex (MgADP or MnADP); curve 6, MF1 preincubated in the buffer at 37 °C for 5 min with a large excess (2.5 mM) of $MgSO_4$ followed by 2.2 μM ADP. Afterward, F_1 samples were diluted up to 15 nM in the spectrophotometer cell to measure the ATPase activity in the presence of 100 μM ATP as the substrate, in a buffer containing 20 mM Tris/HCl at pH 7.4, 4 mM $MgCl_2$, and an ATP regenerating system, as described in the Materials and Methods.

according to ref *26* in a buffer containing 100 mM Tris/SO_4, 4 mM EDTA, and glycerol 50% (v/v) at pH 8. The enzyme fractions with $A_{280}/A_{260} > 1.9$, which contain less than 0.2 mol of nucleotides per mol of MF1, were collected, precipitated in ammonium sulfate at 50%, and stored at 4 °C.

The enzyme purity and the small subunits stoichiometric composition were determined by SDS−PAGE *(27)*.

Activity Measurements. The activity measurements were performed as described in ref *28*. A total of 2.2 μM stripped MF1 was pelletted by centrifugation and dissolved at room temperature in a buffer containing 20 mM Tris/HCl and 20% (v/v) glycerol at pH 7.4. Different samples were analyzed: (1) MF1 preincubated in the buffer at 37 °C for 15 min without added metal and nucleotides, (2 and 3) MF1 preincubated in the buffer at 37 °C for 5 min with 2.2 μM metal (Mg^{2+} or Mn^{2+}), followed by incubation for 10 min with added 2.2 μM ADP, (4 and 5) MF1 preincubated in the buffer at 37 °C for 15 min with 2.2 μM metal−ADP complex (MgADP or MnADP), and (6) MF1 preincubated in the buffer at 37 °C for 5 min with a large excess (2.5 mM) of $MgSO_4$ followed by 2.2 μM ADP (see Figure 1).

Afterward, MF1 samples were diluted up to 15 nM in the spectrophotometer cell for measuring the ATPase activity under trisite conditions, i.e., in the presence of 100 μM ATP as the substrate in a buffer containing 20 mM Tris/HCl at pH 7.4, 4 mM $MgCl_2$, and an ATP-regenerating system (1.5 mM phosphoenolpyruvate, 1 mM KCl, 1 unit/mL of pyruvate kinase, 1 unit/mL of lactate dehydrogenase, and 0.3 mM NADH) (*29*). The reaction was monitored by observing the disappearance of NADH absorbance at 340 nm until a steady-state rate was obtained. The activity was calculated in the initial and final steady-state phases using an extinction coefficient of 6.22 mM cm^{-1}.

EPR Samples Preparation. A sample of stripped MF1 was centrifuged, and the pellet was suspended at room temperature in 20 mM HEPES-KOH and 20% glycerol (v/v) buffer at pH 8.

The sample for EPR analysis had a final volume of 100 μL, and stripped F1 had a final concentration of 35 μM. Mn^{2+} (sulfate salt) freshly prepared or single nucleotides dissolved in 20 mM HEPES-KOH buffer at pH 8 or Mn^{2+}−nucleotide complexes were added using a few microliters of millimolar concentration solutions, and the sample was immediately frozen in liquid nitrogen until the EPR spectra were recorded. If the metal and nucleotide solutions were sequentially added, a preincubation for 5 min with Mn^{2+} was performed before the addition of stoichiometric or 10 times more concentrated nucleotide solution.

EPR Measurements. Pulsed ESEEM experiments were all carried out using an X-band ESP380 Pulse EPR Bruker spectrometer, equipped with a dielectric resonator. The measurements were performed at 4 K using an Oxford C935 liquid helium flow cryostat and an Oxford ITC4 temperature controller. A three-pulse ESEEM sequence was used to get the echo decays (*30*), and the proper phase cycle was applied to eliminate contribution from spurious echoes (*31*). The delay time τ between the first two pulses was chosen as 120 or 144 ns, depending on the field setting, to maximize the ^{31}P peak intensity and minimize the free proton frequency signal. Moreover, experiments with delay times τ of 160, 200, and 240 ns were performed to avoid blind-spot effects, which could possibly hide signals from different magnetic nuclei, as ^{14}N (*32*). The time T between the second and third pulse was varied in a step of 8 ns, and 400 points were recorded, starting with the initial time $T_i = 80$ ns.

The recorded time decays were processed for dead-time correction both with algorithm of Mims (*33*) and with the LPSVD method (*34*); both methods provided similar reconstructed spectra. The application of two different algorithms was used as a double check to verify the correctness of the reconstruction. After dead-time reconstruction, the echo decays were Fourier-transformed to produce ESEEM spectra in the frequency domain.

The HF-EPR spectra were obtained at about 95 and 190 GHz at the National High Magnetic Field Laboratory in Tallahassee (FL) with a homemade spectrometer (*35*). This machine is built around a superconducting magnet with a 17 T "main" coil and a ±0.1 T "sweep" coil (Oxford Instruments Inc.). The source, which has been used in this study, is a Gunn oscillator emitting in the 92−98 GHz range and equipped with a Schottky diode harmonic generator for obtaining higher frequencies (ABmm, Paris, France). The operating microwave frequency is measured with and frequency locked to a source locking microwave counter (EIP 578B from EIP Microwave Inc., Milpitas, CA).

The spectrometer was used in its basic configuration ("single pass" transmission mode) that uses oversized-cylindrical waveguides for propagation of the microwave power. The transmission probe is in a liquid helium flow cryostat of the dynamic type (CF 1200 from Oxford Instruments Inc.); the temperature is monitored within ±0.1 degree. We used a liquid-helium-cooled In-Sb "hot electron" bolometer (QMC Instruments, Cardiff, U.K.).

The spectra were obtained by modulation of the magnetic field at a frequency of 20 kHz with modulation amplitude

Table 1: ZFS Parameter *D*, *E*/*D* Ratio, and ^{55}Mn Hyperfine Coupling, A_{iso}, of the Samples Studied with HF-EPR

	molar ratio of MF1/ nucleotide/Mn^{II}	*D* (mT)	*E*/*D*	A_{iso} (mT)
MF1 + Mn^{II}	1:1:1	20[a]	0.3[b]	9.56 ± 0.03
Mn^{II}MF1 + ADP	1:1:1	20[a]	0.3[b]	9.56 ± 0.03
MF1 + Mn^{II}ADP	1:1:1	38[a]	0.25[a]	9.55 ± 0.03
Mn^{II}MF1 + AMPPNP	1:1:1	43[a]	0.1[a]	9.43 ± 0.03
MF1 + Mn^{II}AMPPNP	1:1:1	35[a]	0.3[a]	9.43 ± 0.03

[a] Estimated error of 10%. [b] Estimated error of 20%.

of 0.2−0.4 mT and in the temperature range of 10−20 K. The main coil was in persistent mode, and the magnetic field changed by variation of the additional field of the sweep coil.

Spectra at 190 GHz were recorded to verify that the spectral features in the 95 GHz spectra are only due to high-order effects of the ZFS interaction and not to different metal sites (*23*). If the line splitting is a consequence of the ZFS broadening, then it should be reduced as the frequency increases from 95 to 190 GHz. The spectra recorded at 190 GHz did not show line splitting, thus confirming that only one Mn^{2+} site is present in the protein samples and that there is no free Mn^{2+} ion in solution.

General analysis of EPR spectra from high spin ($S = {}^5/_2$, $I = {}^5/_2$) Mn^{II} complexes have already been published in various articles (for instance, see refs *18* and *36*). In this study, our analysis is related to experimental data taken at 95 and 190 GHz; thus, a perturbation theoretical treatment to the third order of the Mn^{II} hyperfine and ZFS interactions is fully sufficient to describe our Mn^{II} HF-EPR spectra (*19*). Numerical data analysis was done by a computer program written in Matlab. The program is based on perturbation theory as described by Reed and Markham (*18*). It allows the fitting of the experimental spectra by means of manual simulations by variation of the independent parameters, given by the ZFS parameters *D* and *E* and the Mn^{II} hyperfine coupling. An inhomogeneous line width of 4−5 G (*18*) was used to account for the small hyperfine couplings of metal-coordinated magnetic nuclei (^{31}P and ^{1}H). The simulations were obtained using either a single set of *D* and *E* values and a Gaussian distribution in *D* with a half-width of 20 or 40 G, as reported in the figures. This last procedure did not significantly improve the spectral fitting.

RESULTS

Inhibition of ATPase Activity by the Divalent Metal and ADP or Divalent Metal−ADP Complex. To have evidence that the subunit, which interacts with stoichiometric Mn^{2+}, is one catalytic β subunit, inhibition experiments using Mg^{2+}/Mn^{2+} and ADP were performed in condition of trisite catalysis, which is obtained by adding saturating ATP (see the activity measurements). Figure 1 shows that incubation of stripped MF1 with Mg^{2+} and ADP (1:1), added sequentially or together as a preformed complex, induces the generation of the Mg^{II}ADP-inhibited form upon induction of trisite catalysis (compare curves 2 and 4 with curve 1); i.e., ATP is hydrolyzed with a low initial rate, which increases during turnover to reach an uninhibited steady-state rate. More specifically, in the first 100 s, during which the Mg^{II}ADP inhibition is evident, the curve slope is decreased by about 30% with respect to the steady-state rate

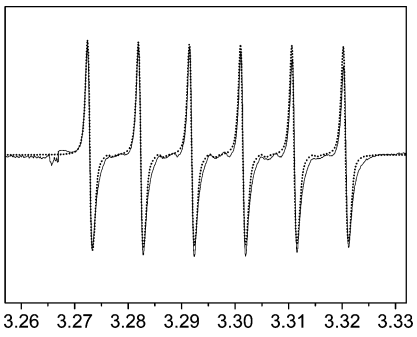

FIGURE 2: W-band EPR spectrum ($T = 20$ K) of Mn^{II}MF1 with simulation (···). Simulation was performed with a Gaussian distribution in *D* with a half-width of 2.0 mT.

(second part of the curve). The same degree of inhibition was developed when the enzyme was treated with Mn^{2+} instead of Mg^{2+} (curves 3 and 5 overlapped to curves 2 and 4), suggesting that even at low concentrations these cations bind the β subunit adopting the same final conformation (i.e., β_{ADP}).

The inhibitory effect is magnified (55% inhibition of the curve slope) when MF1 is pretreated with saturating Mg^{2+} and a stoichiometric amount of ADP (compare curve 1 and 6) according to Frasch et al. (*37*), who propose that such an effect is a result of the free Mg^{2+} binding at the other sites when the inhibitory Mg^{II}ADP is already bound.

EPR and ESEEM Measurements. We have recorded the EPR and ESEEM spectra of the MF1 + Mn^{II} sample and of different MF1(0,0) preparations, obtained by loading the protein with stoichiometric Mn^{II} and stoichiometric or excess amounts of ADP or AMPPNP. Mn^{II} and nucleotides were added to MF1(0,0) either subsequently or together as preformed complexes. We will present separately the results obtained on preparations containing ADP or AMPPNP. The high-field CW-EPR spectra recorded at the W band (95 GHz) for the samples reported in Table 1 are shown in Figures 2−4 together with their simulations. The simulations of the HF-EPR spectra provided the ZFS parameters, *D* and *E*, and the Mn^{II} hyperfine coupling collected in Table 1. For the samples, MF1 + Mn^{II}ADP, Mn^{II}MF1 + AMPPNP, and MF1 + Mn^{II}AMPPNP, the previous parameters were obtained by the simultaneous fitting of the 95 and 190 GHz EPR spectra.

X-band CW-EPR powder spectra of Mn^{II} complexes are quite complicated because the ZFS interaction introduces higher order effects and forbidden transitions in the spectral pattern, for example, see Figure 5, in which the X-band EPR spectrum of MF1 + Mn^{II} sample at 20 K is reported. The X-band EPR spectra of the other protein samples show similar line-shape broadening. At high magnetic fields, the higher order effects of the ZFS interaction are almost

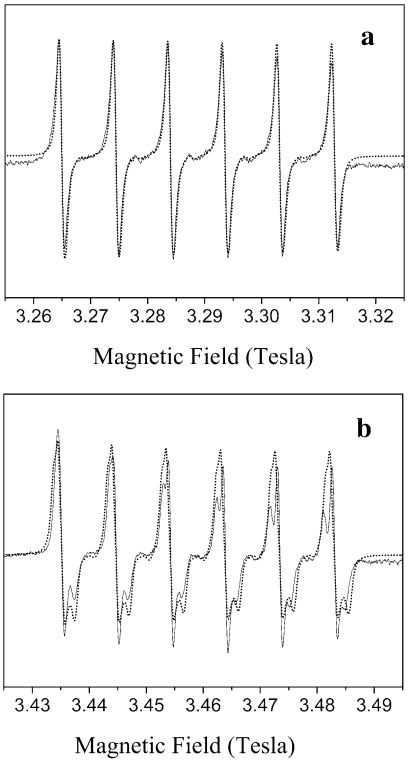

FIGURE 3: W-band EPR spectra ($T = 20$ K) of (a) Mn^{II}MF1 + ADP and (b) MF1 + Mn^{II}ADP with simulations (···). Simulations were performed with a Gaussian distribution in *D* with a half-width of 2.0 mT.

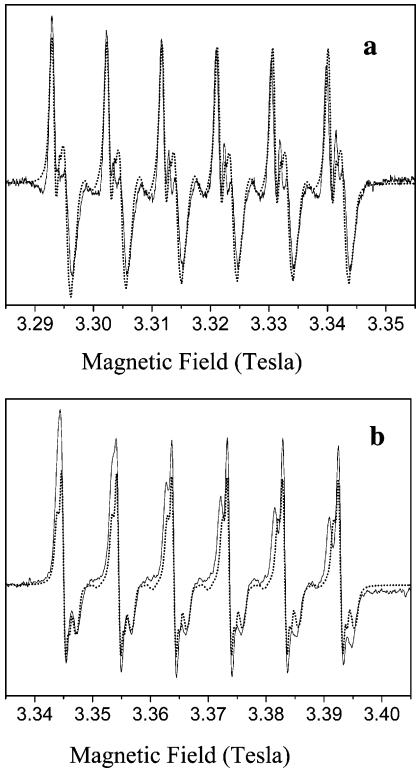

FIGURE 4: W-band EPR spectra ($T = 20$ K) of (a) Mn^{II}MF1 + AMPPNP and (b) MF1 + Mn^{II}AMPPNP with simulations (···). Simulations were performed with a Gaussian distribution in *D* with a half-width of 4.0 mT (a) and 2.0 mT (b).

suppressed and the spectra become considerably simpler to interpret and simulate. At the W band, only the transitions $M_S = -1/2 \leftrightarrow +1/2$ are observed and the spectrum consists of six lines, because of the hyperfine coupling with the ^{55}Mn $I = 5/2$ nucleus. Each line is anisotropically broadened by the ZFS interaction, which affects the $-1/2 \leftrightarrow +1/2$ transitions to the second and third order. Because of this effect, simulations of HF-EPR spectra make it possible to get the ZFS parameters *D* and *E* related to the metal−ligand coordination. In particular, the local coordination symmetry is paramount in determining the ZFS tensor values.

MF1 + Mn^{II} Sample. The HF-EPR spectrum of the MF1 + Mn^{II} sample (Figure 2) shows ZFS parameters $|D| \approx 20$ mT and $|E| \approx 7$ mT.

The *D* parameter is small when compared with other Mn^{2+} sites in proteins (*18*). The overall distortion from the perfect cubic symmetry is not significant as inferred from the low *D* value, while the deviation from the axial symmetry is very pronounced because of the *E/D* ratio reaching the maximum value of $1/3$.

Mn^{2+} in H_2O/glycerol (80:20 weight ratio) solution (same solvent used for the protein samples) shows ZFS parameters very similar to those of MF1 + Mn^{II}. However, the CW-EPR spectra both at the X and W band recorded for the two samples in the same experimental conditions, in the temperature range 10−20 K, present very different microwave saturation behavior. While the spectra of Mn^{2+} in water/glycerol do not saturate even at high microwave power, in the presence of MF1, the EPR spectra can be saturated very easily, indicating less efficient spin-lattice relaxation processes because of higher rigidity of the metal-coordination site in the protein (data not shown) (*38*).

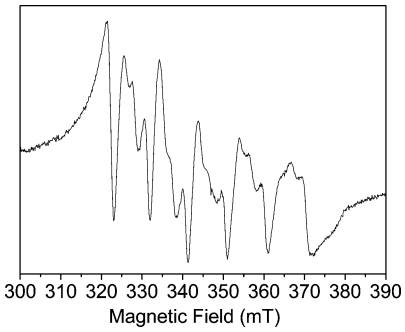

FIGURE 5: X-band EPR spectrum ($T = 20$ K) of Mn^{II}MF1.

A deeper insight in the coordination around the Mn^{2+} can be obtained from three-pulse ESEEM spectra. The MF1 + Mn^{II} FT ESEEM spectrum recorded at $B_0 = 327.8$ mT is shown in Figure 6B. The intense peak at about 14.0 MHz corresponds to the free proton frequency. The broad peaks at 10.4 and 17.4 MHz and the shoulder at about 13.0 MHz shift with the magnetic field as the proton frequency. To check if these features are due to protons coupled to the Mn^{II} ion, we performed simulations of the three-pulse echo decay following the procedure reported in ref *44*, which takes into account the contributions of nuclear transitions in all of the electron spin manifolds of the high-spin Mn^{II} ion. In Figure 6A, we report the experimental echo decay (trace a) along with the simulation obtained by considering only the frequencies of free ^{1}H and ^{14}N nuclei (trace c) and the simulation obtained by including a coupled proton with an axial hyperfine tensor (trace b). The FT of both the calculated echo decays is reported in Figure 6B. It is evident that the experimental time and frequency profiles are reproduced better by considering the coupled proton (traces b). The

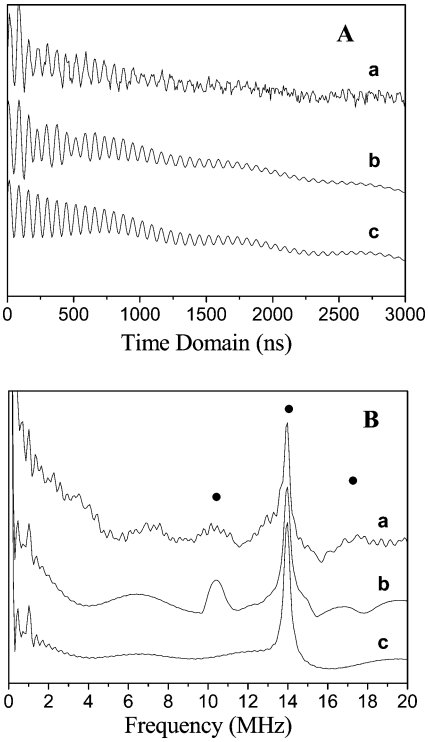

FIGURE 6: (A) ESEEM spectrum (trace a) in the time domain of Mn^{II}MF1. Experimental parameters: magnetic field = 327.8 mT; microwave frequency = 9.70 GHz; shot repetition time = 5.12 ms; τ = 120 ns; pulse length = 16 ns; data points = 400; step = 8 ns. Trace b, simulation obtained by taking into account free ^{1}H and ^{14}N Larmor frequencies and a coupled proton with a = 0.8 MHz and $|T_\perp|$ = 3.4 MHz. All of the electron spin transitions of the $S = {}^5/_2$ Mn ion were considered. It was necessary to introduce a modulation at the free Larmor frequency of the ^{14}N to better reproduce the experimental trace. Trace c, simulation obtained by considering only the modulation at Larmor frequencies of free ^{1}H and ^{14}N nuclei. (B) Traces a−c are the traces a−c of A after dead-time reconstruction (LPSVD method) and Fourier transformation. In trace a, the proton peaks are indicated with a dot. In trace b, a slight broadening of the 10.2 MHz component was introduced to better reproduce the experimental profile.

simulation has been obtained using the hyperfine parameters determined in ref *43* for the protons of water molecules in the $[Mn(H_2O)_6]^{2+}$ complex in water/glycerol frozen solution (isotropic coupling A_{iso} = 0.8 MHz and perpendicular component of the dipolar tensor $|T_\perp|$ = 3.4 MHz). This hyperfine coupling is similar to that found in many biological and inorganic systems (*22*, *39*−*42*), where Mn^{2+} is directly coordinated to water molecules.

^{1}H peaks similar to those observed for the MF1 + Mn^{II} sample are present also in the ESEEM spectra of all of the other protein samples, with added nucleotides that we have examined. The intensities of these peaks are strongly dependent on the field position at which the ESEEM spectrum is taken and on the chosen delay time τ in the echo sequence.

It has to be noted that the echo decay in Figure 6A can be well-reproduced only by also taking into account the free ^{14}N frequency. This fact is a further indication that the Mn^{2+} ion is coordinated to the protein, because this frequency is present for paramagnetic centers in a nitrogen-rich environment. However, in the ESEEM spectra of the MF1 + Mn^{II} sample, there is no evidence of nitrogen nuclei directly coupled to the Mn^{2+} ion.

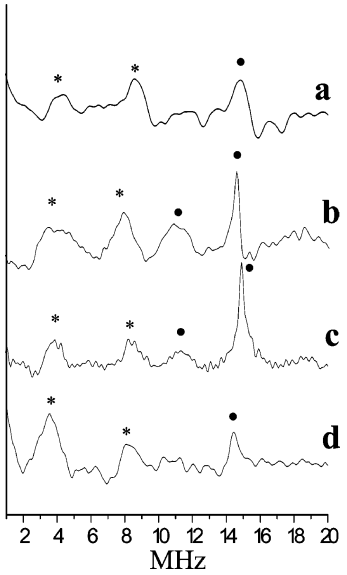

FIGURE 7: ESEEM spectra (T = 4 K) of (a) MF1 + Mn^{II}ADP (1:1) (b) Mn^{II}MF1 + ADP (1:1) (c) Mn^{II}MF1 + ADP (1:10) (d) MF1ADP + Mn^{II} (1:10:1). The asterisks indicate the ^{31}P peaks and the dots indicate ^{1}H peaks. Experimental parameters: shot repetition time = 5.12 ms; pulse length = 16 ns; τ = 144 ns; data points = 400; and step = 8 ns. (a) Magnetic field = 346.3 mT, and microwave frequency = 9.67 GHz. (b) Magnetic field = 346.3 mT, and microwave frequency = 9.67 GHz. (c) Magnetic field = 349.2 mT, and microwave frequency = 9.75 GHz. (d) Magnetic field = 337.3 mT, and microwave frequency = 9.75 GHz.

MF1 + Mn^{II}ADP, Mn^{II}MF1 + ADP, Mn^{II}MF1 + ADP (1:10), and MF1 + ADP + Mn^{II} (1:10:1) Samples. HF-EPR spectra have been recorded for the first two samples in which Mn^{2+}, MF1, and ADP were equimolar. The spectra shown in Figure 3 present marked differences indicating different Mn^{II}−ligand coordination symmetry. Mn^{II}MF1 + ADP shows a very similar spectrum (Figure 3a) to that of the MF1 + Mn^{II} sample without added nucleotides (see Figure 2); the ZFS parameters obtained by spectra simulation indicate rhombic local symmetry but little overall distortion (low D value). ZFS parameters similar to those obtained for MF1 + Mn^{II} and Mn^{II}MF1 + ADP were determined from Q-band EPR spectra for a metal-depleted CF1 sample supplemented with Mn^{2+} (Mn/CF1 ratio = 0.3). In this latter sample, approximately one ADP molecule remains bound to CF1 (*14*).

On the contrary, the MF1 + Mn^{II}ADP sample (Figure 3b) presents a D value about double the value of the Mn^{II}MF1 + ADP sample; this indicates a much stronger overall distortion of the metal site from the cubic symmetry if the preformed Mn^{II}ADP complex is added to the protein.

The ESEEM spectra of the four samples containing ADP are shown in Figure 7. Besides the free proton peak, all of the spectra show resonances ascribable to ^{31}P coupling, two peaks (marked with asterisks in the figure) approximately placed about the free ^{31}P nuclear frequency (ν_P = 5.95 MHz at B_0 = 345.0 mT) moving with the field setting as the free phosphorus frequency. The two peaks form a pattern very similar to that reported for other Mn^{II}−nucleotide systems (*14*, *45*), and they can be attributed to the interaction of the Mn^{2+} with the ^{31}P nuclei of the phosphate ligand of ADP. The peak frequencies and line shapes are different for each of the four samples. Spectra of MF1 + Mn^{II}ADP (Figure 7a) are very weak with splitting of 4.6 ± 0.1 MHz. Table 2

Table 2: ^{31}P Hyperfine Coupling Constants, as Determined by ESEEM

	molar ratio of MF1/nucleotide/Mn^{II}	^{31}P HCC (MHz)
Mn^{II}MF1 + ADP	1:1:1	4.2 ± 0.1
MF1 + Mn^{II}ADP	1:1:1	4.6 ± 0.1
Mn^{II}MF1 + ADP (1:10)	1:10:1	4.45 ± 0.10
MF1 + ADP + Mn^{II} (1:10:1)	1:10:1	4.50 ± 0.10
Mn^{II}MF1 + AMPPNP	1:1:1	4.6 ± 0.1
MF1 + Mn^{II}AMPPNP	1:1:1	4.6 ± 0.1
Mn^{II}MF1 + AMPPNP (1:10)	1:10:1	4.6 ± 0.1

collects the ^{31}P hyperfine coupling measured in all of the samples that we studied. When ADP is added to the protein after adding the Mn^{2+} ion (Mn^{II}MF1 + ADP sample), the ESEEM peaks are more intense and much broader (Figure 7b). The average ^{31}P hyperfine coupling is 4.20 ± 0.1 MHz, significantly reduced with respect to the coupling of the sample in which the preformed Mn^{II}ADP complex is added to the protein.

If ADP is added to the MF1 + Mn^{II} complex in a 10:1 molar ratio [Mn^{II}MF1 + ADP (1:10) sample, Figure 7c], the peaks are narrower than in the previous case and the ^{31}P hyperfine coupling becomes larger, $A = 4.45 \pm 0.1$ MHz, a value within the couplings of the first two samples.

The last sample, MF1 + ADP + Mn^{II} (1:10:1), with ADP added to the protein in a 10:1 molar ratio before adding the Mn^{2+} ion, shows a similar pattern but with broader peaks (Figure 7d). The ^{31}P coupling is $A = 4.50 \pm 0.1$ MHz, very close to that measured for the previous sample, in which ADP was added to the complex MF1 + Mn^{II} in molar ratio of 10:1.

MF1 + Mn^{II}AMPPNP, Mn^{II}MF1 + AMPPNP, and Mn^{II}MF1 + AMPPNP (1:10) Samples. The HF-EPR spectra of Mn^{II}MF1 + AMPPNP and MF1 + Mn^{II}AMPPNP are reported in Figure 4. When these spectra are compared with the MF1 + Mn^{II} HF-EPR spectrum (Figure 2), striking differences are evident, which provide clear indication of different Mn^{2+} ligand environments in the three samples. The samples with added nucleotides show similar *D* values, almost two times the *D* value obtained for the MF1 + Mn^{II} complex. However, the two samples show very different *E/D* values, in particular, in Mn^{II}MF1 + AMPPNP, the *E/D* ratio is very small and thus the coordination site of the Mn^{2+} ion approaches axial symmetry. The other sample, in which the preformed complex Mn^{II}AMPPNP is added to the protein, has an *E/D* ratio close to the maximum value of $^1/_3$. This *E/D* value together with the high *D* parameter points to a coordination site with highly distorted rhombic symmetry.

The ESEEM spectra of the three samples with AMPPNP added to the protein are shown in Figure 8. They are recorded at very similar magnetic fields (see the caption). Besides the peak at the free proton frequency, the spectra contain two peaks at about 4.0 and 8.5 MHz, which can be attributed to ^{31}P couplings. The peak splitting is 4.6 ± 0.1 MHz and remains almost unchanged in the three samples.

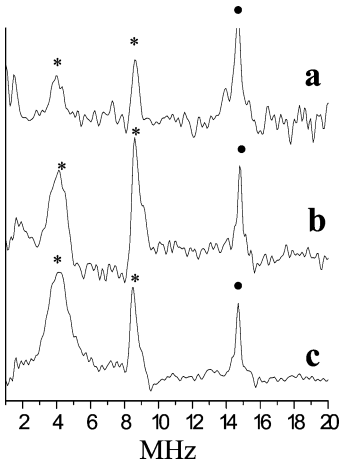

FIGURE 8: ESEEM spectra ($T = 4$ K) of (a) MF1 + Mn^{II}AMPPNP (1:1), (b) Mn^{II}MF1 + AMPPNP (1:1), and (c) Mn^{II}MF1 + AMPPNP (1:10). The asterisks indicate the ^{31}P peaks and the dots indicate ^{1}H peaks. Experimental parameters: shot repetition time = 5.12 ms; pulse length = 16 ns; $\tau = 120$ ns, data points = 400; and step = 8 ns. (a) Magnetic field = 345.0 mT, and microwave frequency = 9.66 GHz. (b) Magnetic field = 347.9 mT, and microwave frequency = 9.69 GHz. (c) Magnetic field = 345.2 mT, and microwave frequency = 9.75 GHz.

DISCUSSION AND CONCLUSION

As mentioned in the Introduction, EPR and ESEEM techniques have been previously applied to study the metal-coordination site(s) in F_1 from thermophilic bacterium PS3 (TF1) and from chloroplast (CF1). Although TF1 and CF1 are highly homologous with MF1, the enzymes from different sources show different metal−nucleotide dependence. For example, TF1 is stable and fully active in the absence of bound nucleotides (*4*). To be fully active, isolated MF1 must contain three tightly bound nucleotides, and their depletion gives MF1(0,0), which is highly unstable in the absence of high concentrations of glycerol (*2*, *46*). Purified CF1 is catalytically inactive and can be activated by depletion of the ϵ subunit and reduction of disulfides of the γ subunit. Latent CF1 contains only four metal−nucleotides, two of which are bound with high affinity to catalytic sites (sites 1 and 4) and two to noncatalytic sites (sites 2 and 5). Only activated CF1 binds the metal−nucleotide also in the low-affinity site 3 (*11*).

CF1, differently depleted from Mg^{2+} and nucleotides, was extensively studied by Frasch et al. (*11*, *12*, *37*, *47*), by means of EPR techniques and substitution of Mg^{2+} with VO^{2+}. The lower affinity metal sites were exhaustively investigated, in particular, the catalytic site 3, identified as corresponding to site β_E in MF1, which was studied both in the protein-latent form and upon activation. The EPR techniques appeared very valuable in identifying different species related to changes in the site conformation because of the replacement of an equatorial ligand induced by the protein activation. The involved amino acids were identified by mutagenesis and ESEEM spectra of the mutants (*37*, *47*). The same approach allowed for the identification in activated CF1 of the metal ligands when nucleotide−ADP was bound to the high-affinity catalytic site, corresponding to site β_{DP} of MF1 (*12*).

MF1 + Mn^{II} Sample. The spectrum shown in Figure 6 demonstrates that no lysine nitrogen is involved in the Mn^{2+}-binding site on MF1, because in the ESEEM spectra, only couplings to protons of coordinated water molecules are apparent. This is in accordance with the MF1 crystal structure, which shows no nitrogen close to the catalytic binding site (*2*). Conversely, in previous studies on stripped TF1, it was demonstrated that Mn^{2+}, added in a stoichio-

metric amount, presents a nitrogen ligand, which was proposed as ϵ-NH_2 of β-Lys164 (*14*).

No direct comparison is possible between our results on MF1 and CF1 because, as already discussed, no experiment exists on this latter protein stripped of nucleotides.

In addition, CF1 containing 0.14 Mg^{2+} and 0.75 ± 0.25 ADP was studied in ref *14* by adding to the protein Mn^{2+} in different cation/protein ratios. In the 0.8:1.0 sample, the ESEEM spectra showed a ^{31}P coupling from a phosphate group of the endogenous ADP, but no peaks ascribable to nitrogen interaction were detected. Instead, in the Mn^{2+} complexes with higher Mn^{2+}/CF1 ratios, $^{14}N-$metal interaction was found and was interpreted as a result of the filling, at higher Mn^{2+} content, of additional metal-binding sites, these latter involving ^{14}N donors. These results are somewhat comparable with our results on MF1, in which no $^{14}N-$metal interaction has been found in the high-affinity metal site, both in the absence and in the presence of nucleotides. It has to be noted that very different EPR and ESEEM results were obtained by the same authors on analogous CF1 preparations using VO^{2+} instead of Mn^{2+} as a paramagnetic cation (*13*).

MF1Mn^{II} + Nucleotide and MF1 + Mn^{II}nucleotide Samples. In samples obtained by preloading the stripped MF_1 with Mn^{2+} and later adding stoichiometric ADP, the initial metal-site symmetry is not modified by the nucleotide binding, because the ZFS values *D* and *E* are identical to those found for the MF1 + Mn^{II} sample (Table 1). The nucleotide is surely coordinated to the Mn^{2+} because peaks due to the interaction with ^{31}P nuclei occur in the ESEEM spectra.

In the following analysis of the ESEEM spectra, we will focus mainly on peak distances, because of the difficulty to account for line shapes and line widths.

The ESEEM spectra of MF1 + Mn^{II} after addition of 10 times ADP (Figure 7c) show narrower peaks and larger ^{31}P hyperfine coupling owing to some conformational change. In fact, the larger coupling is related to a shorter distance between the interacting spins localized on the metal ion and on the ^{31}P nucleus or to an increase in the $Mn^{II}-O-P$ angle (*41*); moreover, the minor peak broadening can be related to a reduced dispersion in the $Mn^{II}-^{31}P$ distances and/or in the $Mn^{II}-O-P$ angles. Similar spectral features pointing to the same conformational effect are obtained by preloading the stripped enzyme with 10 times ADP before stoichiometric addition of Mn^{2+} (Figure 7d). These results are in agreement with previous findings that ADP excess induces the enzyme to adopt a closer structure as a consequence of the filling of catalytic and regulatory binding sites (*48*). The HF-EPR spectra of the two samples with a large excess of ADP were not recorded, but their X-band spectra confirm the ESEEM results. In fact, the spectra of these latter samples are very similar to each other but different from the X-band spectra of samples with ADP added to the protein in a 1:1 ratio.

In the sample obtained by adding the preformed Mn−ADP complex to MF1, the *D* and *E* parameters are very different from those of the previous sample, in which Mn^{2+} and ADP were sequentially added to the enzyme (see Table 1). In both samples, the ESEEM spectra show interactions between the metal and the nucleotide phosphate(s), although the measured ^{31}P couplings are different. The coupling is significantly smaller when ADP is added to the MF1 + Mn^{II} complex, and these data can be related to a larger distance (i.e., looser binding) between the metal and nucleotide when ADP is sequentially added. All of these observations clearly demonstrate a different approach of the metal to the enzyme, when the metal is isolated or bound to ADP in the Mn^{II}ADP complex. It has to be noted that, according to the literature, ADP surely binds the enzyme in the P loop, which enfolds the phosphate moieties in the nucleotide-binding sites β-Lys164 and β-Thr165 (*2*, *49*).

When the enzyme works in trisite catalysis, our kinetic data indicate that the sequence of addition to the protein of the divalent cation and ADP does not influence the final conformation of a competent catalytic site, because the same ATP hydrolysis rate, both in the initial inhibited and final steady-state phases, is observed (Figure 1). This indicates that two different states of the same β catalytic site occur before catalysis starts (precatalytic states); these states are monitored in frozen solutions by the EPR spectra.

Unlike addition of ADP, the adding of AMPPNP to the preformed MF1 + Mn^{II} complex leads to a dramatic modification of the metal-site symmetry as a consequence of the triphosphate nucleotide binding. The site acquires a quasi-axial symmetry but with a much higher overall cubic distortion. A higher distortion in the Mg^{2+} site containing AMPPNP with respect to that containing ADP is described by Walker and co-workers in the MF1 crystal (*2*) and interpreted as a result of higher nucleotide affinity for the β_{DP} with respect to the β_{TP} site.

When 10 times more AMPPNP is added to the MF1 + Mn^{II} complex, no significant changes appear in the ESEEM spectra with respect to the 1:1 complex. This is in accordance with the observation that the filling of regulatory and catalytic sites with AMPPNP does not result in the dramatic conformational changes that the excess of ADP induces. (*48*).

If the complex Mn^{II}AMPPNP is added to MF1, the parameters *D* and *E* are very similar to those obtained by adding to the protein the Mn^{II}ADP complex. We checked that the complexes are actually bound to the protein by comparing the HF-EPR spectra obtained for the model complexes $Mn^{II}-$nucleotides in the same solvent (H_2O/glycerol = 80:20). These spectra gave very different ZFS parameters (Mn^{II}ADP, D = 10.0 mT, E = 3.0 mT; Mn^{II}AMPPNP, D = 30.0 mT, E = 8.0 mT) showing a different coordination in the $Mn^{II}-$nucleotide complexes with respect to the ternary complexes obtained by adding the protein. Then, the preformed complexes Mn^{II}ADP and Mn^{II}AMPPNP coordinate the protein with much of the same site symmetry as shown by their similar ZFS parameters. Also, the ^{31}P coupling is similar in the two samples; only the ESEEM line shapes are different, with the peaks of the ADP complex being much broader than those of the AMPPNP complex (Figures 7a and 8a). All of these observations point to a minor ability to approach the protein of the preformed metal−ADP or metal−AMPPNP complexes with respect to the metal alone.

The samples obtained by addition to the protein of the preformed Mn^{II}AMPPNP complex or by sequentially adding Mn^{2+} and AMPPNP show similar *D* but very different *E* parameters (see the Results). Conversely, the ESEEM spectra show similar ^{31}P coupling (see Table 2); there is only some differences in the line shapes, as the progressive broadening of the ν_- peak and the appearance of a shoulder on the ν_+

peak in the MF1 + Mn^{II}AMPPNP sample. These different observations can be rationalized by admitting that the changes in the metal-coordination symmetry are mainly related to nonphosphate ligands. The ^{31}P coordination must be involved very little, because the ^{31}P coupling remains almost unchanged in all of the samples with AMPPNP. The different peak line shapes can be interpreted as the result of slightly more anisotropic coupling in the samples where AMPPNP was added to the protein−Mn^{II} complex.

We stress that in the case of ADP different HF-EPR *and* different ESEEM spectra were obtained for MF1 + Mn^{II}ADP and MF1Mn^{II} + ADP samples. Concerning the ZFS parameters, the difference is mainly in the *D* values (see table); this means that the overall site distortion is much more pronounced in the MF1 + Mn^{II}ADP sample and, because the ^{31}P couplings are also different, the phosphate ligand must be involved in the change of the metal coordination.

We can make a comparison between our results obtained with the MF1 + Mn^{II}ADP and the MF1 + Mn^{II}AMPPNP samples and previous ESEEM and HYSCORE studies on the Mn^{2+} coordination in TF1 (*50*). In this latter work, the samples were prepared by adding, to stripped TF1, the preformed Mn^{II}ADP, Mn^{II}ATP, and Mn^{II}AMPPNP complexes, in a 1:1 ratio. The three-pulse ESEEM spectra of these samples showed peaks due to coupling between Mn^{2+} and ^{31}P nuclei, but differences were present, depending on the bound nucleotide. In the samples containing ADP and ATP, the two ^{31}P ESEEM peaks showed different phosphorus couplings. Moreover, in the TF1 + Mn^{II}AMPPNP sample, the ν_+ peak appeared structured, suggesting metal coupling with two ^{31}P nuclei. The HYSCORE spectra supported this interpretation for the samples containing ATP and AMPPNP, because the contour peaks showed an elongated shape resulting from the presence of two correlations. Conversely, our ESEEM spectra show similar ^{31}P coupling in both samples containing ADP and AMPPNP, although in the ADP sample, the peaks are broader, indicating a more anisotropic coupling and/or a dispersion in the Mn^{II}−nucleotide binding geometry. In the case of AMPPNP, we cannot say if the ESEEM peaks can derive from metal coupling with one or two ^{31}P from the nucleotide phosphates. Unfortunately, our samples gave very weak echo signals, preventing the acquisition of HYSCORE spectra. On the other hand, in ref *50*, it was also observed that metal coordination to only one ^{31}P could not be excluded on the basis of the relatively weak ESEEM signals of the samples containing ATP and AMPPNP. In this alternative interpretation, the complex line shape of the HYSCORE spectra could reflect the anisotropy of the hyperfine interaction.

By using EPR techniques and kinetic inhibition analysis, we were able to verify that (1) Mn^{2+} added in a 1:1 ratio to MF1(0,0) enters one catalytic site on one β subunit. (2) The preloading of MF1(0,0) with Mn^{2+} triggers the high-affinity conformation of the catalytic site, so that subsequent adding of stoichiometric amount of nucleotides induces selective loading of the site containing the metal ion. ADP or AMPPNP binding results in changes of the metal coordination, which are more dramatic in the case of the triphosphate nucleotide. Regarding this aspect, our data agree with the results obtained by Burgard et al. *(51)*, who used EPR spectroscopy and a spin-labeled ATP analogous to investigate the effects of Mg^{2+} ions on the structure of the nucleotide-binding sites in MF1 and TF1. They found that the Mg^{2+} ions not only influence the nucleotide binding to F_1, but also alter the structure and geometry of the nucleotide-binding site. This compares well with the results of our study that, in a direct way, using a paramagnetic cation probe instead of a labeled nucleotide probe, provides evidences of the importance of the cation binding in preforming the nucleotide-binding site in stripped MF1. Moreover, like in the investigation of Burgard et al. (*51*), which revealed differences between MF1 and TF1 in the structure of the nucleotide-binding sites, we obtained, regarding the Mn^{2+} binding to the stripped MF1, different results with respect to those previously obtained in a similar TF1 preparation (*14*). (3) The direct loading of MF1(0,0) with preformed Mn^{II}ADP or Mn^{II}AMPPNP gives similar Mn^{2+} coordination geometries, which differ from those obtained by adding sequentially the Mn^{2+} cation and the nucleotide. However, in the case of stoichiometric ADP, the different EPR spectra are probably an indication of two functional precatalytic conformations. Upon induction of the trisite catalytic cycle, the latter conformations give rise to the same final metal−ADP-inhibited form of the enzyme, as a result of the entrapment of metal−ADP at the high-affinity site. In addition, the filling by the excess of ADP of the catalytic and noncatalytic sites of MF1 (preloaded or not with stoichiometric Mn^{2+}) similarly affects the two EPR species. Both results confirm the role of "cross-talk" between the different nucleotide-binding sites (*2*). (4) By studying protein samples prepared in different ways, we were able to prove for MF1 what Senior et al. (*52*) and Frasch (*11*) have demonstrated for respectively *E. coli* F1 and CF1: the active role of the divalent cation in creating a competent catalytic site upon binding.

HF CW-EPR and ESEEM techniques appear to be very sensitive and suitable spectroscopic methods for conformational studies of MF1 in frozen solution, after replacing the natural cation Mg^{2+} with paramagnetic divalent metals. The presence of a metal−nucleotide in only one catalytic site slows down the transitions through different protein rearrangements, making it possible to observe by EPR techniques the induced conformations, with the advantage of using proteins in solution. The geometries that we observed with stoichiometric metal−nucleotide could mimic the functional states of the high-affinity catalytic site during the unisite cycle.

To elucidate the geometry of the metal−nucleotide complex bound to the high-affinity site related to functional conformations of the trisite catalysis, experiments on the enzyme fully loaded with metal−nucleotides are underway.

REFERENCES

1. Walker, J. E. (1994) The regulation of catalysis in ATP synthase, *Curr. Opin. Struct. Biol. 4* (6), 912−918.
2. Abrahams, J. P., Leslie, A. G. W., Lutter, R., and Walker, J. E. (1994) Structure at 2.8 Å resolution of F_1-ATPase from bovine heart mitochondria, *Nature 370*, 621−628.
3. Walker, J. E., Fearnley, I. M., Gay, N. J., Gibson, B. W., Northrop, F. D., Powell, S. J., Runswick, M. J., Saraste, M., and Tybulewicz, V. L. (1985) Primary structure and subunit stoichiometry of F_1-ATPase from bovine mitochondria, *J. Mol. Biol. 184* (4), 677−701.
4. McCarty, R. E. (1992) A plant biochemist's view of proton-ATPases and ATP synthases, *J. Exp. Biol. 172*, 431−441.
5. Kagawa, Y. (1999) Biophysical studies on ATP synthase, *Adv. Biophys. 36*, 1−25.

6. Berger, G., Girault, G., and Zimmermann, J. L. (1998) Cooperativity between the enzymatic sites of F_1-ATPase revisited by the use of HPLC methods, *J. Bioenerg. Biomembr. 30* (6), 543−553.
7. Reynafarje, B. D., and Pedersen, P. L. (1996) ATP synthase−Conditions under which all catalytic sites of the F1 moiety are kinetically equivalent in hydrolyzing ATP, *J. Biol. Chem. 271* (51), 32546−32550.
8. Weber, J., Hammond, S. T., Wilke-Mounts, S., and Senior, A. E. (1998) Mg^{2+} coordination in catalytic sites of F_1-ATPase, *Biochemistry 37* (2), 608−614.
9. Weber, J, Wilke-Mounts, S., and Senior, A. E. (1994) Cooperativity and stoichiometry of substrate binding to the catalytic sites of *Escherichia coli* F_1-ATPase. Effects of magnesium, inhibitors, and mutation, *J. Biol. Chem. 269* (32), 20462−20467.
10. Selwyn, M. J. (1968) Model reaction for mitochondrial adenosine triphosphatase, *Nature 219* (153), 490−493.
11. Frasch, W. D. (2000) The participation of metals in the mechanism of the F_1-ATPase, *Biochim. Biophys. Acta 1458* (2 and 3), 310−325.
12. Chen, W., Hu, C. Y., Crampton, D. J., and Frasch, W. D. (2000) Characterization of the metal binding environment of catalytic site 1 of chloroplast F_1-ATPase from *Chlamydomonas*, *Biochemistry 39* (31), 9393−9400.
13. Zimmermann, J. L., Schneider, B., Morlet, S., Amano, T., and Sigalat, C. (2000) The role of the Mg^{2+} cation in ATP synthase studied by electron paramagnetic resonance using VO^{2+} and Mn^{2+} paramagnetic probes, *Spectrochim. Acta, Part A 56* (2), 285−299.
14. Buy, C., Girault, G., and Zimmermann, J. L. (1996) Metal binding sites of H^+-ATPase from chloroplast and *Bacillus* PS3 studied by EPR and pulsed EPR spectroscopy of bound manganese(II), *Biochemistry 35* (30), 9880−9891.
15. Chernyak, B. V., and Cross, R. L. (1992) Adenine nucleotide-binding sites on mitochondrial F_1-ATPase: Studies of the inactive complex formed upon binding ADP at a catalytic site, *Arch. Biochem. Biophys. 295* (2), 247−252.
16. Jault, J. M., and Allison, W. S. (1994) Hysteretic inhibition of the bovine heart mitochondrial F_1-ATPase is due to saturation of noncatalytic sites with ADP which blocks activation of the enzyme by ATP, *J. Biol. Chem. 269* (1), 319−325.
17. (1993) EMR of Paramagnetic Molecules, in *Biological Magnetic Resonance* (Berliner, L. J., and Reuben, J., Eds.) Vol. 13, Plenum Press, New York.
18. Reed, G. H., and Markham, G. D. (1984) EPR of Mn(II) Complexes with Enzymes and Other Proteins, in *Biological Magnetic Resonance* (Berliner, L. J., and Reuben, J., Eds.) Vol. 6, pp 73−142, Plenum Press, New York.
19. Rohrer, M., Prisner, T. F., Brügmann, O., Käss, H., Spoerner, M., Wittinghofer, A., and Kalbitzer, H. R. (2001) Structure of the metal-water complex in Ras·GDP studied by high field EPR spectroscopy and ^{31}P NMR spectroscopy, *Biochemistry 40* (7), 1884−1889.
20. Espe, M. P., Hosler, J. P., Ferguson-Miller, S., Babcock, G. T., and McCracken, J. (1995) A continuous wave and pulsed EPR characterization of the Mn^{2+} binding site in *Rhodobacter sphaeroides* cytochrome *c* oxidase, *Biochemistry 34*, 7593−7602.
21. Gaffney, B. J., Su, C., and Oliw, E. H. (2001) Assignment of EPR transitions in a manganese-containing lipoxygenase and prediction of local structure, *Appl. Magn. Reson. 21*, 411−422.
22. Manikandan, P., Carnieli, R., Shane, T., Kalb(Gilboa), A. J., and Goldfarb, D. (2000) W-band ENDOR investigation of the manganese-binding site of Concanavalin A: Determination of proton hyperfine couplings and their signs, *J. Am. Chem. Soc. 122*, 3488−3494.
23. Arieli, D., Prisner, T. F., Hertel, M., and Goldfarb, D. (2004) Resolving Mn framework sites in large cage aluminophosphate zeotypes by high field EPR and ENDOR spectroscopy, *Phys. Chem. Chem. Phys. 6*, 172−181.
24. Mims, W., and Peisach, J. (1981) Electron Spin-Echo Spectroscopy and the Study of Metalloproteins, in *Biological Magnetic Resonance* (Berliner, L. J., and Reuben, J., Eds.) Vol. 3, pp 213−263, Plenum Press, New York.
25. Lutter, R., Abrahams, J. P., van Raaij, M. J., Todd, R. J., Lundqvist, T., Buchana, S. K., Leslie, A. G. W., and Walker, J. E. (1993) Crystallization of F_1-ATPase from bovine heart mitochondria, *J. Mol. Biol. 229*, 787−790.
26. Garret, N. E., and Penefsky, H. S. (1975) Interaction of adenine nucleotides with multiple binding sites on beef heart mitochondrial adenosine triphosphatase, *J. Biol. Chem. 250*, 6640−6647.
27. Laemmli, U. K. (1970) Cleavage of structural proteins during the assembly of the head of bacteriophage T4, *Nature 277*, 680−685.
28. Daggett, S. G., Gruys, K. J., and Schuster, S. M. (1985) Metal interactions with beef heart mitochondrial ATPase, *J. Biol. Chem. 260* (10), 6213−6218.
29. Rosing, J., Harris, D. A., Kemp, A., and Slater, E. C. (1975) Nucleotide-binding properties of native and cold-treated mitochondrial ATPase, *Biochim. Biophys. Acta 376*, 13−26.
30. Mims, W. B. (1972) Envelope modulation in spin-echo experiments, *Phys. Rev. B 5* (7), 2409−2419.
31. Fauth, J. M., Schweiger, A., Braunschweiler, L., Forrer, J., and Ernst, R. R. (1986) Elimination of unwanted echoes and reduction of dead time in three-pulse electron spin-echo spectroscopy, *J. Magn. Reson. 66*, 74−85.
32. Dikanov, S. A., and Tsvetkov, Y. D. (1992) *Electron Spin-Echo Envelope Modulation (ESEEM) Spectroscopy*, CRC Press, Boca Raton, FL.
33. Mims, W. B. (1984) Elimination of the dead-time artifact in electron spin-echo envelope spectra, *J. Magn. Reson. 59*, 291−306.
34. Barkhuijsen, H., de Beer, R., Bovée, W. M. M. J., and van Ormondt, D. (1985) Retrieval of frequencies, amplitudes, damping factors, and phases from time-domain signals using a linear least-squares procedure, *J. Magn. Reson. 61*, 465−481.
35. Hassan, A. K., Pardi, L. A., Krzystek, J., Sienkiewicz, A., Goy, P., Rohrer, M., and Brunel, L. C. (2000) Ultrawide band multifrequency high-field EMR technique: A methodology for increasing spectroscopic information, *J. Magn. Reson. 146*, 300−312.
36. Misra, S. K., and Sun, J. S. (1991) Electron paramagnetic resonance studies of Mn^{2+} in single crystals and powders, *Magn. Reson. Rev. 16*, 57−100.
37. Crampton, D. J., LoBrutto, R., and Frasch, W. D. (2001) Identification of the P-loop lysine as a metal ligand in the absence of nucleotide at catalytic site 3 of chloroplast F_1-ATPase from *Chlamydomonas reinhardtii*, *Biochemistry 40* (12), 3710−3716.
38. Eaton, S. S., and Eaton, G. R. (2000) Relaxation Times of Organic Radicals and Transition Metal Ions, in *Biological Magnetic Resonance* (Berliner, L. J., Eaton, S. S, and Eaton, G. R., Eds.) Vol. 19, pp 29−154, Kluwer Academic/Plenum Publisher, New York.
39. Morrissey, S. R., Horton, T. E., and DeRose, V. J. (2000) Mn^{2+} sites in the hammerhead ribozyme investigated by EPR and continuous-wave Q-band ENDOR spectroscopies, *J. Am. Chem. Soc. 122*, 3473−3481.
40. Zhang, J., and Goldfarb, D. (2000) Mn incorporation into the mesoporous material MCM-41 under acidic conditions as studied by high-field pulsed EPR and ENDOR spectroscopies, *J. Am. Chem. Soc. 122*, 7034−7041.
41. Arieli, D., Delabie, A., Groothaert, M., Pierloot, K., and Goldfarb, D. (2002) The process of Mn(II) incorporation into aluminophosphate zeotypes through high-field ENDOR spectroscopy and DFT calculations, *J. Phys. Chem. B 106*, 9086−9097.
42. Tan, X., Poyner, R., Reed, G. H., and Scholes, C. P. (1993) Electron nuclear double resonance study of the Mn^{2+} environs in the oxalate−ATP complex of pyruvate kinase, *Biochemistry 32*, 7799−7810.
43. Tan, X., Bernardo, M., Thomann, H. and Scholes, C. P. (1993) Pulsed and continuous wave electron double resonance of aquo protons coordinated in frozen solution to high spin Mn^{2+}, *J. Chem. Phys. 98* (7), 5147−5157.
44. Larsen, G. R., Halkides, C. J., and Singel, D. J. (1993) A geometric representation of nuclear modulation effects: The effects of high electron spin multiplicity on the electron spin-echo envelope modulation spectra of Mn^{2+} complexes of N-*ras* p21, *J. Chem. Phys. 98*, 6704−6721.
45. LoBrutto, R., Smithers, G. W., Reed, G. H., Orme-Johnson, W. H., Tan, S. L., and Leigh, J. S., Jr. (1986) Observation of manganese(II)−ligand superhyperfine couplings in complexes with proteins by electron spin-echo spectroscopy, *Biochemistry 25* (19), 5654−5660.
46. Vogel, P. D., and Cross, R. L. (1991) Adenine nucleotide-binding sites on mitochondrial F1-ATPase. Evidence for an adenylate kinase-like orientation of catalytic and noncatalytic sites, *J. Biol. Chem. 266* (10), 6101−6105.

47. Chen, W., and Frasch, W. D. (2001) Interaction of the catch-loop tyrosine bY317 with the metal at catalytic site 3 of *Chlamydomonas* chloroplast F1-ATPase, *Biochemistry 40* (25), 7729−7735.
48. Lippe, G., Di Pancrazio, F., Dabbeni-Sala, F., Bertoli, E., and Tanfani, F. (1995) Influence of ADP, AMP-PNP and of depletion of nucleotides on the structural properties of F1ATPase: A Fourier transform infrared spectroscopic study, *FEBS Lett. 373* (2), 141−145.
49. Weber, J., and Senior, A. E. (2003) ATP synthesis driven by proton transport in F_1F_0-ATP synthase, *FEBS Lett. 545* (1), 61−70.
50. Schneider, B., Sigalat, C., Amano, T., and Zimmermann, J. L. (2000) Evidence for changes in the nucleotide conformation in the active site of H^+-ATPase as determined by pulsed EPR spectroscopy, *Biochemistry 39* (50), 15500−15512.
51. Burgard, S., Nett, J. H., Sauer, H. E., Kagawa, Y., Schafer, H. J., Wise, J. G., Vogel, P. D., and Trommer, W. E. (1994) Effects of magnesium ions on the relative conformation of nucleotide binding sites of F1-ATPases as studied by electron spin resonance spectroscopy, *J. Biol. Chem. 269* (27), 17815−17819.
52. Senior, A. E., Nadanaciva, S, and Weber, J. (2002) The molecular mechanism of ATP synthesis by F_1F_0-ATP synthase, *Biochim. Biophys. Acta 1553*, 188−211.

BI049525K